NIH Public Access
Author Manuscript
Magn Reson Med. Author manuscript; available in PMC 2013 March 1.

Published in final edited form as:
Magn Reson Med. 2012 March ; 67(3): 731–739. doi:10.1002/mrm.23054.

Human Brain Iron Mapping using Atlas-based T_2 Relaxometry

Khader M. Hasan, PhD[1,CA], **Indika S. Walimuni, PhD**[1], **Larry A. Kramer, MD**, and **Ponnada A. Narayana, PhD**[1]

[1]Department of Diagnostic and Interventional Imaging, University of Texas Health Science Center at Houston

Abstract

Several *in vivo* quantitative magnetic resonance imaging (qMRI) techniques have been proposed as surrogate measures to map iron content in the human brain. The majority of *in vivo* qMRI iron mapping methods utilized the age-dependent iron content data based on *postmortem* data. In this work we fused atlas-based human brain volumetry obtained on a large cohort of healthy adults using FreeSurfer with T_2 relaxation time measurements. We provide a brain atlas-based T_2 relaxation time map which was subsequently used along with published *postmortem* iron content data to obtain a map of iron content in subcortical and cortical gray matter. We have also investigated the sensitivity of the linear model relating transverse relaxation rate with published iron content to the number of regions used. Our work highlights the challenges encountered upon using the simple model along with *postmortem* data to infer iron content in several brain regions where *postmortem* iron data are scant (e.g. corpus callosum, amygdale).

Keywords

T2 Relaxation Time; Relaxation Rate; Iron Mapping; Atlas; Human Brain Mapping; FDRI; MFC

Introduction

Iron is present in several complex chemical forms in human brain and is shown to be important in brain tissue metabolism (1–3), but its abnormal accumulation has been implicated in several pathologies (3–6). To date, several quantitative magnetic resonance imaging methods (qMRI) methods were used (1–5) in combination with phantom or postmortem (5–11) measurements to provide *in vivo* surrogate markers of iron content in the human brain. In general, iron mapping methods can be grouped into three categories (3,4): (I) relaxation time (3,8–10,12–18), (II) magnetic field correlation (MFC) which uses asymmetric spin echo (19, 20), and (III) phase-based or susceptibility-weighted methods (3,10,21–24). Relaxation-based methods for iron mapping (3) use spin-lattice relaxation rate ($R_1 = 1/T_1$), or spin-spin relaxation rate ($R_2 = 1/T_2$) or gradient echo methods ($R_2^* = 1/T_2^* = R_2 + R_2'$), where T_2 and T_1 are the transverse and longitudinal relaxation times, respectively. An important relaxation rate based method is the field dependent R_2 increase method (FDRI) in which R_2 measurements are performed on the same subjects at two magnetic fields ($\mathbf{B_0}$) (24–26).

Several investigations (see Table 5 in Ref. 3) have shown that R_1 (3, 13, 14), R_2 (3, 8, 9, 10, 12, 15, 16, 18), R_2^* (3, 8, 12, 17) or R_2' ($R_2' = R_2^* - R_2$) correlated strongly with brain

[CA]Corresponding Author: Khader M. Hasan, Ph.D., Associate Professor of Diagnostic and Interventional Imaging, Department of Diagnostic and Interventional Imaging, University of Texas Health Science Center at Houston, 6431 Fannin Street, MSB 2.100, Houston, Texas 77030, Tel: Office (713) 500-7690, Fax: (713) 500-7684, Khader.M.Hasan@uth.tmc.edu.

NIH-PA Author Manuscript
NIH-PA Author Manuscript
NIH-PA Author Manuscript

NIH-PA Author Manuscript

NIH-PA Author Manuscript

NIH-PA Author Manuscript

tissue iron content using histological or postmortem brain iron measurements (6,8–11). The majority of iron mapping reports to-date used the caudate, putamen, and globus pallidus, as representative of extrapyramidal gray matter structures (3). Langkammer at al. (10) and Gelman et al. (15) showed that both R_2 and R_2' correlated with iron content while Vymazal et al. (14) showed that R_1 and R_2 correlated with iron content. Hikita et al. (16) reported that both R2' and R2 can be used for mapping iron in the basal ganglia, but since R_2' is affected by macroscopic magnetic field inhomogeneity, R_2 was recommended for iron mapping. Several other works reported strong correlation between R_2 with iron (see Table 5 in Ref 3).

Phase sensitive or susceptibility-weighted imaging (SWI) methods have also been used to map iron (3,11,22–24). In two recent reports, phase sensitive methods did not correlate with iron content compared with R_2* (11) or FDRI methods (24).

We are not aware of a unified model (2) that can be used to explain the apparent paradox of iron correlation with R_1, R_2, R_2*, R_2' and FDRI measurements as reported in the literature.

Compared to gradient-echo methods, the R_2 maps are less sensitive to macroscopic field inhomogeneities and are computationally less intensive compared to other methods (16). In this work we used spin-echo measurements with long repetition time to obtain regional R_2 values. This work has two major goals. First, we present the regional heterogeneity of T2 relaxation values on subcortical, deep and cortical gray matter in addition to deep and lobar white matter using atlas-based anatomical labels. Second, we attempt to correlate our R_2 measurements at 3.0 T with iron content using the *postmortem* age vs. iron content data reported in 1958 by Hallgren and Sourander (6). To verify the validity of the R_2 relaxation rate approach used in this report as a surrogate marker of iron, we also demonstrate the association between other *in vivo* qMRI methods such as MFC (20) and FDRI (26) and between published FDRI and R_2 measurements using *in vivo* brain atlas-based methods.

Materials and methods

Participants

This retrospective study has been approved by our institutional review board and is fully compliant with the Health Insurance Portability and Accountability Act (HIPAA). A written informed consent was obtained from each participant prior to data acquisition. All participants were neurologically normal based on the review of medical history. All scans were read as "normal" by a board certified radiologist. The participants included 86 right-handed healthy adults with 42 males (age range = 18.7–56.8 years; mean age ± SD = 35.4 ± 10.3 years) and 44 females (age range = 19.0–56.0; mean age ± SD = 37.2 ± 9.8 years).

MRI Data Acquisition

We acquired whole-brain conventional MRI (T1-weighted and dual spin-echo) data using a Philips 3.0 T Intera system with a dual quasar gradient system with a maximum gradient amplitude of 80 mT/m, maximum slew rate of 200 mT/m/ms and an eight-channel SENSE compatible head coil (Philips Medical Systems, Best, Netherlands).

T1-weighted data

T1-weighted data were acquired using 3D fast field-echo sequence (3D-FFE) with a field-of-view (FOV) of 240 × 240 mm^2 and isotropic voxel size of 0.9375 mm covering the entire brain. The flip angle, repetition time (TR), echo time (TE), and scan time were 6°, 10.3 ms, 2.0 ms and 322 sec, respectively.

NIH-PA Author Manuscript

NIH-PA Author Manuscript

NIH-PA Author Manuscript

T2-weighted data

T2-weighted data acquired using 2D dual turbo spin-echo (TSE) sequence with scan time ~ 367 seconds, $TE_1/TE_2/TR$=8/90/6800 ms in the axial plane (3mm slice thickness, square FOV = 240x240 mm^2 at 44 axial sections).

Processing

A pictorial flowchart of the computational procedures applied to the MRI data is illustrated in Fig. 1. The MRI data processing pipeline used in this work is described in more details elsewhere (27).

Segmentation and Parcellation of T1-weighted Data

The T1-weighted brain data were automatically segmented into cortical and sub-cortical regions using FreeSurfer software library (28; http://surfer.nmr.mgh.harvard.edu/). Using the cortical and sub-cortical segmentations provided by FreeSurfer (28, 29), an atlas consisting of about hundred and eighty white matter (WM), gray matter (GM), and cerebrospinal fluid (CSF) regions was generated for each subject in the T1-weighted native space (29). A tabulation of the brain anatomical labels (non-CSF) provided by FreeSurfer and used in this work is provided in the Supplementary Table. Due to its complex structure and poor white and gray matter contrast on T1-weighted data, the thalamus segmented by FreeSurfer contained both white and gray matter.

Computation of Relaxation Time from Dual Spin Echo Data

The T_2 relaxation times were estimated from the early and late echoes (TE_1, TE_2) volumes according to standard spin-echo procedures assuming a single compartment model (30,31):

$$S_i = k * PD * \left(1 - \exp\left(-\frac{TR}{T_1}\right)\right) * \exp\left(-\frac{TE_i}{T_2}\right) \quad [1]$$

where S_i is the signal intensity of the *i*th echo; the T_2 relaxation time is obtained as (30, 31):

$$T_2 = \frac{TE_2 - TE_1}{\ln\left(\frac{S(TE_1)}{S(TE_2)}\right)} \quad [2]$$

Fusion of T2 Relaxation Time and T1-weighted Data

The T_2 relaxation time map for each subject was registered to the T1-weighted data using advanced normalization tools (ANTs) with symmetric normalization (32). The ANTs tool has also been independently tested and compared against 14 different registration programs (33). A detailed description of the methods used in the registration is presented previously (27). Since the T1-weighted volume and the brain atlas are in the same space, the atlas was used as a look-up table to locate chosen brain structures from all other image modalities registered to the T1-weighted space.

Brain iron concentration using Hallgren and Sourander Postmortem data

As described in the Introduction, several previous reports (3,12–18,22–26) have used the *postmortem* (6) best fit age vs. regional brain iron content data to estimate iron content using *in vivo* qMRI surrogates such as R_1 (13, 14), R2* (12, 15), and R_2 (15, 18) relaxation rates. In brief, regional iron content for each of the 12 brain regions (r) in Hallgren and Sourander (6) was estimated for each subject (n) as function of age using Equation [3]:

NIH-PA Author Manuscript

NIH-PA Author Manuscript

NIH-PA Author Manuscript

$$Iron(n,r)=A(r)*(1-\exp(-B(r)*Age(n)))+C(r) \quad [3]$$

Statistical analysis

Age comparisons between males and females were conduced using independent t-test. Regional comparisons in R_2 and estimated iron content were evaluated using paired t-tests applied to compare qMRI data obtained from the entire cohort on several related regions (e.g. motor and sensory cortex). The t-test results on two variables as used in this work are equivalent to one way analysis-of-variance ($F = t^2$). The correlations between regional R_2 and iron content using the Hallgren and Sourander postmortem data (6) or the published MFC and FDRI data were computed using the Pearson correlation coefficient (32). All statistical analyses were performed using MATLAB R12.1 Statistical Toolbox v 3.0 (The Mathworks, Natick, MA).

Results

The healthy men and women in our cohort did not differ in age (p=0.40, F=0.72). Given previous reports of insignificant gender-based differences in brain volumetry (35) and to simplify the analyses we group-averaged microstructural brain data obtained from age-matched men and women used in this study bilaterally.

Quantification and Visualization of T_2 Relaxation Time

Table 1 summarizes the group average volume and corresponding T_2 relaxation time of 28 white and gray matter regions that cover the entire human brain subcortical, cortical GM, deep and lobar white matter. Table 2 covers 12 additional cortical and lobar regions such as prefrontal, visual, motor and sensory cortices and corresponding white matter lobes. We included the prefrontal, motor and sensory regions as iron content data were provided in the Hallgren and Sourander post mortem study (6) and these functionally important cortical subdivisions could be looked up in our brain atlas. The qMRI average and standard deviation were obtained by volume-weighted averaging of the corresponding brain atlas labels or subvolumes tabulated in Supplemenray Table. Figure 2 shows a multiview of the T_2 relaxation time map (Fig. 2A) at a level selected for visualizing the basal ganglia, cerebral cortex, corpus callosum, amygdale and hippocampus.

The T_2 relaxation time average values (Table 2; Table 3; Fig 2A) are smallest in the globus pallidus (T_2 =66.9 ± 3.3 ms) whereas the largest T_2 values are measured in the frontal gray matter (T_2 =134.9 ± 8.1 ms). The lobar white matter T_2 values are significantly smaller than the corresponding cortical gray matter (e.g. T_2(occipital cortex) > T_2(occipital white matter); $p<1\times10^{-20}$; F=839). The average T_2 values in the occipital cortex are significantly smaller than the average values in the parietal cortex ($p<1\times10^{-20}$; F=937). The average T_2 values in the motor precentral cortex of the frontal lobe (T_2 =135.6 ± 10.7 ms) are significantly smaller than the average values (T_2 =138.54 ± 11.1 ms) in the sensory postcentral cortex of the parietal lobe ($p=1\times10^{-7}$; F=34). The average T_2 values in the hippocampus are significantly greater than that in the amygdala ($p<1\times10^{-20}$; F=187). The deep periventricular (non-callosal) white matter T_2 relaxation time values are significantly smaller than the average values in the caudate ($p<1\times10^{-20}$; F =355). Note that the T_2 relaxation time is significantly smaller in the anterior (genu) CC compared with the posterior (splenium) CC (p=0.0002; F=15).

NIH-PA Author Manuscript

NIH-PA Author Manuscript

NIH-PA Author Manuscript

Estimation of Iron Content FDRI and MFC in our cohort

The A, B and C parameters in Equation [3] were obtained from (6) to estimate the iron content in 12 brain regions for each subject in our cohort. The iron content mean and standard deviation on our cohort is provided in Table 3 along with the corresponding R_2 values from Table 2 and Table 3. To compare the methods (see section below), Table 3 includes the estimated average and standard deviation FDRI values on our cohort. The FDRI values were estimated using the ROI-based age vs. FDRI best linear fit parameters tabulated in Bartzokis et al. (26) on 8 regions that included the hippocampus, genu and splenium of the corpus callosum. Note that the postmortem iron content data in Hallgren and Sourander did not include these three regions. Table 3 also includes the average normative MFC values reported by Ge et al. (20) on six brain regions that did not include the caudate.

Correlation between our R_2 and Iron Measurements

Using the tabulated parameters in Table 3, we conducted a linear regression analysis of the volume-averaged and atlas-based R_2 measurements vs. the iron content on some selected groups of regions listed in Table 1 and Table 2 (regression model: $R_2 = \alpha + \beta^*[\text{Iron}]$). Table 4 provides the intercept (α), slope (β) and the corresponding Pearson correlation coefficient (r) and statistical significance (p) of several possible comparisons of the data in Table 3. Using the 12 regions including thalamus and frontal white matter the correlation coefficient between R_2 and iron was significant (r =0.906; p=0.00005).

Consistent with several previous reports (12,14,15), the thalamus (12) and frontal white matter measurements clearly deviated from the best fit upon visual inspection of the data. After removing the thalamus and frontal white matter measurements (Table 4), the correlation between iron content and R_2 became stronger ($R_2 = (6.444 \pm 0.412) + (0.042 \pm 0.005)^*$ [Iron]); r=0.951, p=0.00002). To test the sensitivity of these results due to the number of regions included, Table 4 provides some results using 5, 7, 8 and 9 regions. Note that excluding the three brain regions with the highest iron content (i.e. globus, putamen and caudate) resulted in statistically insignificant correlations (r=0.168, p=0.72).

Visual Representation of Extrapolated Brain Iron Content

Using the best linear fit parameters obtained on the first 10 regions excluding frontal white matter and thalamus (Table 4), we inferred the regional iron content using the measured R_2 values in all gray matter structures assuming the linear relationship [Iron] = $(-131.40 \pm 23.42) + (21.36 \pm 2.46) * R_2$. The group-averaged brain iron content map is presented in Fig. 2b. The iron concentration is shown in units of part-per-million (ppm) or (μg [Fe]/g wet weight) allowing the presentation of the scalar and positive iron content output data in bytes (range 0 – 255). Figure 2b shows the iron content values of several gray matter regions that were not included in Hallgren and Sourander (6). For example, our data shows that the amygdale contains higher iron concentration (60.07 ± 5.92 μg [Fe]/g wet weight) than the hippocampus (49.83 ±7.39 μg [Fe]/g wet weight) ($p<1\times10^{-20}$; F = 203).

Comparison between FDRI, MFC, R_2 and estimated Iron Content

Table 4 provides the linear regression analyses results (intercept, slope, standard deviations, correlation coefficient and significance) of the estimated iron content, estimated FDRI, published control MFC and our R_2 measurements as summarized in Table 3. The correlation between FDRI and R_2 measurements was significant (r = 0.865; p= 0.006) using the 8 structures including thalamus, frontal WM. The FDRI vs. R_2 correlation was stronger upon excluding our caudate measurements (r=0.959; p=0.00066). Our R_2 measurements also correlated strongly with the normative MFC values (r=0.995; p=0.000035). The estimated

NIH-PA Author Manuscript

NIH-PA Author Manuscript

NIH-PA Author Manuscript

FDRI and published normative MFC measurements correlated strongly (r=0.997; p=0.00016; see Table 4).

Discussion

To the best of our knowledge, this is the first human brain atlas-based report of age-extrapolated iron content of the cortical gray matter. We presented the spatial heterogeneity of water T_2 relaxation time on a large cohort of healthy adults. We adopted FreeSurfer for atlas-based volume measurements (28, 35). Our methods adapted validated procedures to fuse and register microstructral MRI metrics such as T_2 relaxation time with high resolution T1-weighted atlases in each subject native space (27). We presented subcortical, cortical gray matter, deep and lobar white matter to illustrate spatial and interregional heterogeneity. To verify our R_2-based results, we have also contrasted our approach with two alternative qMRI methods that were used to provide markers of brain iron such as FDRI and MFC. We found strong correspondence between published MFC and FDRI methods on one hand, and a strong association between the current R_2 approach and the FDRI approach, on the other hand. We tabulated the volume of each brain region used as our quantitative measurements are averaged over the entire brain region volume (12,30,31). This is important when comparing our findings with previous reports that adopted ROI (14–16,18), or voxel-based approaches (12).

The relative average values of the normative adult brain volumes in our work (e.g. frontal cortex > temporal > occipital > putamen > caudate > hippocampus> amygdala) are consistent with several volumetric reports using manual delineation or automated methods (12,30,35). We have used dual fast spin echo and adopted a single compartment model to estimate the T_2 relaxation time in both gray and white matter. The primary contribution of this work pertains to the heterogeneity of T_2 relaxation time measurements in gray matter and their potential as a marker for iron content using atlas-based methods.

In accordance with previous reports (30,31,36–38), we found significant region-dependent variations in transverse T_2 relaxation (T_2: globus pallidus < putamen < white matter < cortex). Consistent with a recent atlas-based study on healthy adults (30), the average T_2 relaxation time of the occipital cortical gray matter was significantly smaller than the temporal, frontal and parietal cortices (T_2: occipital < temporal < parietal < frontal). Our finding of significantly smaller average T_2 relaxation time in the precentral motor cortex compared to the postcentral sensory cortex is concordant with increased iron in the motor cortex compared with the sensory cortex as reported by Hallgren and Sourander (6). The finding of relatively low iron content in the hippocampus compared to the subcortical gray matter regions is consistent with previous MRI (8,26) and postmortem data (3,7).

Consistent with previous reports on the regional heterogeneity of the corpus callosum using T_2 relaxation time measurements (36,39,40), our data indicate that T_2 relaxation time values of the anterior CC are significantly smaller than that of the posterior CC (Fig. 2a). This inter-regional T_2 relaxation trend on the CC has also been reported using T_1 relaxation times (e.g. T_1(gCC) < T_1(sCC); see 36). The observation that T_2(gCC) < T_2(sCC) could not be explained exclusively by myelin since the anterior CC has been shown in human adult postmortem samples to be populated by slow-conducting, thin and lightly myelinated axons (41). In addition, the myelin water content of the genu has been shown to be significantly smaller than in the splenium (36).

This paradoxical result on the CC indicates that other biophysical factors in addition to myelin may contribute to the measured T2 relaxation time in compact white matter with reduced myelin. In our simple single compartment model we ignored the possible

NIH-PA Author Manuscript

NIH-PA Author Manuscript

NIH-PA Author Manuscript

contribution of fast exchange between free water molecules in the genu with a potentially short-lived macomolecular pool (42–44). Therefore, exchange of water with this "solid-like" compartment would reduce the effective T_2 relaxation time measured using the two echoes (42).

A relatively larger iron content in the frontal CC than the posterior CC would offer another plausible explanation to this finding on the corpus callosum. To the best of our knowledge, there has been no comprehensive histopathological report (11) on the iron content of the different and functionally specialized subdivisions of the human CC. Scant postmortem data available indicate that the iron content of the CC is low (8–10). Higher iron content in the genu of the CC compared to the splenium CC may be inferred from the FDRI and MFC data (see Table 3; Table 4).

The iron content contribution to white matter relaxation rate has been debated (17, 18). A recent study by Li et al. (17) did not report strong association between iron content and relaxation rate in compact white matter tracts.

In this work, we presented the mean age and volume-averaged iron map of deep and cortical gray matter excluding the thalamus proper and frontal white matter. We noted along with previous reports (12,14,15,18,19) that white matter R_2 measurements deviated from the iron vs. R_2 inter-regional best least-squares fit. We applied a linear model relating R_2 and iron content to gray matter measurements and used as many regions we could match using our atlas labels with published data (6). In a recent report, Mitsumori et al. (18) adapted a model proposed by Gelman et al. (45) that incorporated the macromolecular fraction (e.g. 1 – free water fraction) to account for deviant R_2 measurements in white matter (e.g. $R_2 = \alpha + \beta *$ iron $+ \gamma * (1 -$ water fraction)). In a future extension of this work, other regional microstructural qMRI metrics such as the diffusivities obtained using diffusion tensor imaging will be examined in addition to the water content.

This retrospective study has several limitations. The R_2 relaxation rate approach used in our work as an *in vivo* surrogate marker of iron depended on *postmortem* measurements from an important study published in 1958 which did not include detailed information about gender, handedness, side and the exact location of the ROIs used. Brain structures such as hippocampus, amygdale and the corpus callosum subdivisions were not included (6). As noted in the Results (see Table 4), the approach adopted in this work to estimate iron was not sensitive upon excluding brain structures with the highest iron content. However, to the best of our knowledge, ours is the first to use 10–12 regions to obtain the best linear regression fit parameters (Table 4); almost all previous iron mapping studies used 3–9 regions (3,11,12) that included identifiable regions with high iron content such as putamen and globus palllidus.

The application of iron mapping methods may be challenged if water distribution and tissue microsture are altered and produce counter effects that reduce the relaxation rate sensitivity to iron (46). For example, natural aging may increase water content in the extracellular space and neuronal cells would decrease in size while iron may also increase in gray matter (5,31,46). If demyelination of white matter occurs due to aging (31), or pathology (47,48), T_2 may increase, but commensurate iron deposition due to pathology (6) would decrease T_2. In these scenarios, the measured relaxation rate may not be a direct and specific marker of iron (3,46). The presence of blood deposits (e.g. traumatic injury) gliosis (48,49), and microcalcifications in the volume-of-interest may also confound the measured relaxation rate (1,5).

The single compartment model adopted in this work could not separate the relative contributions from the intracellular and extracellular compartments in gray matter. The

NIH-PA Author Manuscript

NIH-PA Author Manuscript

NIH-PA Author Manuscript

application of the single compartment model to white matter can not separate the intra-axonal, myelin water, extracellular and the semisolid macromolecular pool (50–54). To improve the specificity of relaxation measurements the acquisition of additional MRI contrasts (56–58) at different echo times and using multicompartment models would allow objective analysis of the sensitivity and specificity of different iron mapping methods.

Additional histopathological and *in situ* standardized quantitative MRI measurements of key human brain structures such as amgydala, hippocampus, visual, motor and sensory cortices, anterior and posterior CC are needed to help isolate or model the *in vivo* contributors to MRI microstructural metrics (2,3). In conclusion, our results underscore the utility of using standardized multimodal and atlas-based approaches and the need for sophisticated models to understand the yet unresolved biophysical contributors to MRI signal.

Supplementary Material

Refer to Web version on PubMed Central for supplementary material.

Acknowledgments

This work is funded by the National Institutes of Health NIH/NINDS R01-NS052505-04 and Dunn Research Foundation to K.M.H, and NIH/NIBIB EB002095 to P.A.N. The purchase of the 3.0 T MRI clinical scanner is partially funded by NIH grant S10 RR19186 awarded to P.A.N. We wish to thank Vipul Kumar Patel for helping in data acquisition.

References

1. Schenck JF, Zimmerman EA. High-field magnetic resonance imaging of brain iron: birth of a biomarker? NMR Biomed. 2004; 17:433–445. Review. [PubMed: 15523705]
2. Gossuin Y, Muller RN, Gillis P. Relaxation induced by ferritin: a better understanding for an improved MRI iron quantification. NMR Biomed. 2004; 17:427–432. Review. [PubMed: 15526352]
3. Haacke EM, Cheng NY, House MJ, Liu Q, Neelavalli J, Ogg RJ, Khan A, Ayaz M, Kirsch W, Obenaus A. Imaging iron stores in the brain using magnetic resonance imaging. Magn Reson Imaging. 2005; 23:1–25. [PubMed: 15733784]
4. Stankiewicz J, Panter SS, Neema M, Arora A, Batt CE, Bakshi R. Iron in chronic brain disorders: imaging and neurotherapeutic implications. Neurotherapeutics. 2007; 4:371–386. [PubMed: 17599703]
5. Drayer B, Burger P, Darwin R, Riederer S, Herfkens R, Johnson GA. Magnetic resonance imaging of brain iron. Am. J. Roentgenol. 1986; 147:103–110. [PubMed: 3487201]
6. Hallgren B, Sourander P. The effect of age on the non-haemin iron in the human brain. J. Neurochem. 1958; 3:41–51. [PubMed: 13611557]
7. Deibel MA, Ehmann WD, Markesbery WD. Copper, iron, and zinc imbalances in severely degenerated brain regions in Alzheimer's disease: possible relation to oxidative stress. J Neurol Sci. 1996; 143:137–142. [PubMed: 8981312]
8. Thomas LO, Boyko OB, Anthony DC, Burger PC. MR detection of brain iron. AJNR Am J Neuroradiol. 1993; 14:1043–1048. [PubMed: 8237678]
9. House MJ, St Pierre TG, McLean C. 1.4T study of proton magnetic relaxation rates, iron concentrations, and plaque burden in Alzheimer's disease and control postmortem brain tissue. Magn Reson Med. 2008; 60:41–52. [PubMed: 18523986]
10. Langkammer C, Krebs N, Goessler W, Scheurer E, Ebner F, Yen K, Fazekas F, Ropele S. Quantitative MR imaging of brain iron: a postmortem validation study. Radiology. 2010; 257:455–462. [PubMed: 20843991]
11. Yao B, Li TQ, Gelderen P, Shmueli K, de Zwart JA, Duyn JH. Susceptibility contrast in high field MRI of human brain as a function of tissue iron content. Neuroimage. 2009; 44:1259–1266. [PubMed: 19027861]

NIH-PA Author Manuscript

NIH-PA Author Manuscript

NIH-PA Author Manuscript

12. Peran P, Hagberg G, Luccichenti G, Cherubini A, Brainovich V, Celsis P, Caltagirone C, Sabatini U. Voxel-based analysis of R2* maps in the healthy human brain. J Magn Reson Imaging. 2007; 26:1413–1420. [PubMed: 18059009]
13. Ogg RJ, Steen RG. Age-related changes in brain T1 are correlated with iron concentration. Magn Reson Med. 1998; 40:749–753. [PubMed: 9797159]
14. Vymazal J, Righini A, Brooks RA, Canesi M, Mariani C, Leonardi M, Pezzoli G. T1 and T2 in the brain of healthy subjects, patients with Parkinson disease, and patients with multiple system atrophy: relation to iron content. Radiology. 1999; 211:489–495. [PubMed: 10228533]
15. Gelman N, Gorell JM, Barker PB, Savage RM, Spickler EM, Windham JP, Knight RA. MR imaging of human brain at 3.0 T: preliminary report on transverse relaxation rates and relation to estimated iron content. Radiology. 1999; 210:759–767. [PubMed: 10207479]
16. Hikita T, Abe K, Sakoda S, Tanaka H, Murase K, Fujita N. Determination of transverse relaxation rate for estimating iron deposits in central nervous system. Neurosci Res. 2005; 51:67–71. [PubMed: 15596242]
17. Li TQ, Yao B, van Gelderen P, Merkle H, Dodd S, Talagala L, Koretsky AP, Duyn J. Characterization of T(2)* heterogeneity in human brain white matter. Magn Reson Med. 2009; 62:1652–1657. [PubMed: 19859939]
18. Mitsumori F, Watanabe H, Takaya N. Estimation of brain iron concentration in vivo using a linear relationship between regional iron and apparent transverse relaxation rate of the tissue water at 4.7T. Magn Reson Med. 2009; 62:1326–1330. [PubMed: 19780172]
19. Jensen JH, Szulc K, Hu C, Ramani A, Lu H, Xuan L, Falangola MF, Chandra R, Knopp EA, Schenck J, Zimmerman EA, Helpern JA. Magnetic field correlation as a measure of iron-generated magnetic field inhomogeneities in the brain. Magn Reson Med. 2009; 61:481–485. [PubMed: 19161168]
20. Ge Y, Jensen JH, Lu H, Helpern JA, Miles L, Inglese M, Babb JS, Herbert J, Grossman RI. Quantitative assessment of iron accumulation in the deep gray matter of multiple sclerosis by magnetic field correlation imaging. AJNR Am J Neuroradiol. 2007; 28:1639–1644. [PubMed: 17893225]
21. Harder SL, Hopp KM, Ward H, Neglio H, Gitlin J, Kido D. Mineralization of the deep gray matter with age: a retrospective review with susceptibility-weighted MR imaging. AJNR Am J Neuroradiol. 2008; 29:176–183. [PubMed: 17989376]
22. Ogg RJ, Langston JW, Haacke EM, Steen RG, Taylor JS. The correlation between phase shifts in gradient-echo MR images and regional brain iron concentration. Magn Reson Imaging. 1999; 17:1141–1148. [PubMed: 10499676]
23. Xu X, Wang Q, Zhang M. Age, gender, and hemispheric differences in iron deposition in the human brain: an in vivo MRI study. Neuroimage. 2008; 40:35–42. [PubMed: 18180169]
24. Pfefferbaum A, Adalsteinsson E, Rohlfing T, Sullivan EV. MRI estimates of brain iron concentration in normal aging: comparison of field-dependent (FDRI) and phase (SWI) methods. Neuroimage. 2009; 47:493–500. [PubMed: 19442747]
25. Bartzokis G, Aravagiri M, Oldendorf WH, Mintz J, Marder SR. Field dependent transverse relaxation rate increase may be a specific measure of tissue iron stores. Magn Reson Med. 1993; 29:459–464. [PubMed: 8464361]
26. Bartzokis G, Tishler TA, Lu PH, Villablanca P, Altshuler LL, Carter M, Huang D, Edwards N, Mintz J. Brain ferritin iron may influence age- and gender-related risks of neurodegeneration. Neurobiol Aging. 2007; 28:414–423. [PubMed: 16563566]
27. Walimuni IS, Abid H, Hasan KM. A computational framework to quantify tissue microstructural integrity using conventional MRI macrostructural volumetry. Comput Biol Med. 2011
28. Fischl B, Salat DH, Busa E, Albert M, Dieterich M, Haselgrove C, van der Kouwe A, Killiany R, Kennedy D, Klaveness S, Montillo A, Makris N, Rosen B, Dale AM. Whole brain segmentation: automated labeling of neuroanatomical structures in the human brain. Neuron. 2002; 33:341–355. [PubMed: 11832223]
29. Desikan RS, Ségonne F, Fischl B, Quinn BT, Dickerson BC, Blacker D, Buckner RL, Dale AM, Maguire RP, Hyman BT, Albert MS, Killiany RJ. An automated labeling system for subdividing

NIH-PA Author Manuscript

NIH-PA Author Manuscript

NIH-PA Author Manuscript

the human cerebral cortex on MRI scans into gyral based regions of interest. Neuroimage. 2006; 31:968–980. [PubMed: 16530430]

30. Aubert-Broche B, Grova C, Pike GB, Collins DL. Clustering of atlas-defined cortical regions based on relaxation times and proton density. Neuroimage. 2009; 47:523–532. [PubMed: 19426811]
31. Hasan KM, Walimuni IS, Kramer LA, Frye RE. Human brain atlas-based volumetry and relaxometry: application to healthy development and natural aging. Magn Reson Med. 2010; 64:1382–1389. [PubMed: 20740662]
32. Avants BB, Epstein CL, Grossman M, Gee JC. Symmetric diffeomorphic image registration with cross-correlation: evaluating automated labeling of elderly and neurodegenerative brain. Med Image Anal. 2008; 12:26–41. [PubMed: 17659998]
33. Klein A, Andersson J, Ardekani BA, Ashburner J, Avants B, Chiang MC, Christensen GE, Collins DL, Gee J, Hellier P, Song JH, Jenkinson M, Lepage C, Rueckert D, Thompson P, Vercauteren T, Woods RP, Mann JJ, Parsey RV. Evaluation of 14 nonlinear deformation algorithms applied to human brain MRI registration. Neuroimage. 2009; 46:786–802. [PubMed: 19195496]
34. Zou KH, Tuncali K, Silverman SG. Correlation and simple linear regression. Radiology. 2003; 227:617–622. Review. [PubMed: 12773666]
35. Fjell AM, Westlye LT, Amlien I, Espeseth T, Reinvang I, Raz N, Agartz I, Salat DH, Greve DN, Fischl B, Dale AM, Walhovd KB. Minute effects of sex on the aging brain: a multisample magnetic resonance imaging study of healthy aging and Alzheimer's disease. J Neurosci. 2009; 29:8774–8783. [PubMed: 19587284]
36. Whittall KP, MacKay AL, Graeb DA, Nugent RA, Li DK, Paty DW. In vivo measurement of T2 distributions and water contents in normal human brain. Magn Reson Med. 1997; 37:34–43. [PubMed: 8978630]
37. Georgiades CS, Itoh R, Golay X, van Zijl PC, Melhem ER. MR imaging of the human brain at 1.5 T: regional variations in transverse relaxation rates in the cerebral cortex. AJNR Am J Neuroradiol. 2001; 22:1732–1737. [PubMed: 11673169]
38. Kumar R, Delshad S, Macey PM, Woo MA, Harper RM. Development of T2-relaxation values in regional brain sites during adolescence. Magn Reson Imaging. 2010; 29:185–193. [PubMed: 20933351]
39. Bartzokis G, Sultzer D, Lu PH, Nuechterlein KH, Mintz J, Cummings JL. Heterogeneous age-related breakdown of white matter structural integrity: implications for cortical "disconnection" in aging and Alzheimer's disease. Neurobiol Aging. 2004; 25:843–851. [PubMed: 15212838]
40. Kim EY, Kim DH, Yoo E, Park HJ, Golay X, Lee SK, Kim DJ, Kim J, Kim DI. Visualization of maturation of the corpus callosum during childhood and adolescence using T2 relaxometry. Int J Dev Neurosci. 2007; 25:409–414. [PubMed: 17964752]
41. Aboitiz F, Scheibel AB, Fisher RS, Zaidel E. Fiber composition of the human corpus callosum. Brain Res. 1992; 598:143–153. [PubMed: 1486477]
42. Minty EP, Bjarnason TA, Laule C, MacKay AL. Myelin water measurement in the spinal cord. Magn Reson Med. 2009; 61:883–892. [PubMed: 19191283]
43. Levesque IR, Pike GB. Characterizing healthy and diseased white matter using quantitative magnetization transfer and multicomponent T(2) relaxometry: A unified view via a four-pool model. Magn Reson Med. 2009; 62:1487–1496. [PubMed: 19859946]
44. Harrison R, Bronskill MJ, Henkelman RM. Magnetization transfer and T2 relaxation components in tissue. Magn Reson Med. 1995; 33:490–496. [PubMed: 7776879]
45. Gelman N, Ewing JR, Gorell JM, Spickler EM, Solomon EG. Interregional variation of longitudinal relaxation rates in human brain at 3.0 T: relation to estimated iron and water contents. Magn Reson Med. 2001; 45:71–79. [PubMed: 11146488]
46. Hasan KM, Halphen C, Kamali A, Nelson FM, Wolinsky JS, Narayana PA. Caudate nuclei volume, diffusion tensor metrics, and T(2) relaxation in healthy adults and relapsing-remitting multiple sclerosis patients: implications for understanding gray matter degeneration. J Magn Reson Imaging. 2009; 29:70–77. [PubMed: 19097116]

NIH-PA Author Manuscript

NIH-PA Author Manuscript

NIH-PA Author Manuscript

47. Larsson HB, Frederiksen J, Petersen J, Nordenbo A, Zeeberg I, Henriksen O, Olesen J. Assessment of demyelination, edema, and gliosis by in vivo determination of T1 and T2 in the brain of patients with acute attack of multiple sclerosis. Magn Reson Med. 1989; 11:337–348. [PubMed: 2779421]
48. Whittall KP, MacKay AL, Li DK, Vavasour IM, Jones CK, Paty DW. Normal-appearing white matter in multiple sclerosis has heterogeneous, diffusely prolonged T(2). Magn Reson Med. 2002; 47:403–408. [PubMed: 11810687]
49. Neema M, Goldberg-Zimring D, Guss ZD, Healy BC, Guttmann CR, Houtchens MK, Weiner HL, Horsfield MA, Hackney DB, Alsop DC, Bakshi R. 3 T MRI relaxometry detects T2 prolongation in the cerebral normal-appearing white matter in multiple sclerosis. Neuroimage. 2009; 46:633–641. [PubMed: 19281850]
50. Beaulieu C, Fenrich FR, Allen PS. Multicomponent water proton transverse relaxation and T2-discriminated water diffusion in myelinated and nonmyelinated nerve. Magn Reson Imaging. 1998; 16:1201–1210. [PubMed: 9858277]
51. Lancaster JL, Andrews T, Hardies LJ, Dodd S, Fox PT. Three-pool model of white matter. J. Magn. Reson Imaging. 2003; 17:1–10. [PubMed: 12500269]
52. Dyakin VV, Chen Y, Branch CA, Veeranna, Yuan A, Rao M, Kumar A, Peterhoff CM, Nixon RA. The contributions of myelin and axonal caliber to transverse relaxation time in shiverer and neurofilament-deficient mouse models. Neuroimage. 2010; 51:1098–1105. [PubMed: 20226865]
53. Dula AN, Gochberg DF, Valentine HL, Valentine WM, Does MD. Multiexponential T2, magnetization transfer, and quantitative histology in white matter tracts of rat spinal cord. Magn Reson Med. 2010; 63:902–909. [PubMed: 20373391]
54. Ou X, Sun SW, Liang HF, Song SK, Gochberg DF. The MT pool size ratio and the DTI radial diffusivity may reflect the myelination in shiverer and control mice. NMR Biomed. 2009; 22:480–487. [PubMed: 19123230]
55. Ordidge RJ, Gorell JM, Deniau JC, Knight RA, Helpern JA. Assessment of relative brain iron concentrations using T2-weighted and T2*-weighted MRI at 3 Tesla. Magn Reson Med. 1994; 32:335–341. [PubMed: 7984066]
56. Cox EF, Gowland PA. Simultaneous quantification of T2 and T'2 using a combined gradient echo-spin echo sequence at ultrahigh field. Magn Reson Med. 2010; 64:1440–1405. [PubMed: 20593370]
57. Michaeli S, Oz G, Sorce DJ, Garwood M, Ugurbil K, Majestic S, Tuite P. Assessment of brain iron and neuronal integrity in patients with Parkinson's disease using novel MRI contrasts. Mov Disord. 2007; 22:334–340. [PubMed: 17149719]
58. Deoni SC, Rutt BK, Arun T, Pierpaoli C, Jones DK. Gleaning multicomponent T1 and T2 information from steady-state imaging data. Magn Reson Med. 2008; 60:1372–1387. [PubMed: 19025904]

NIH-PA Author Manuscript
NIH-PA Author Manuscript
NIH-PA Author Manuscript

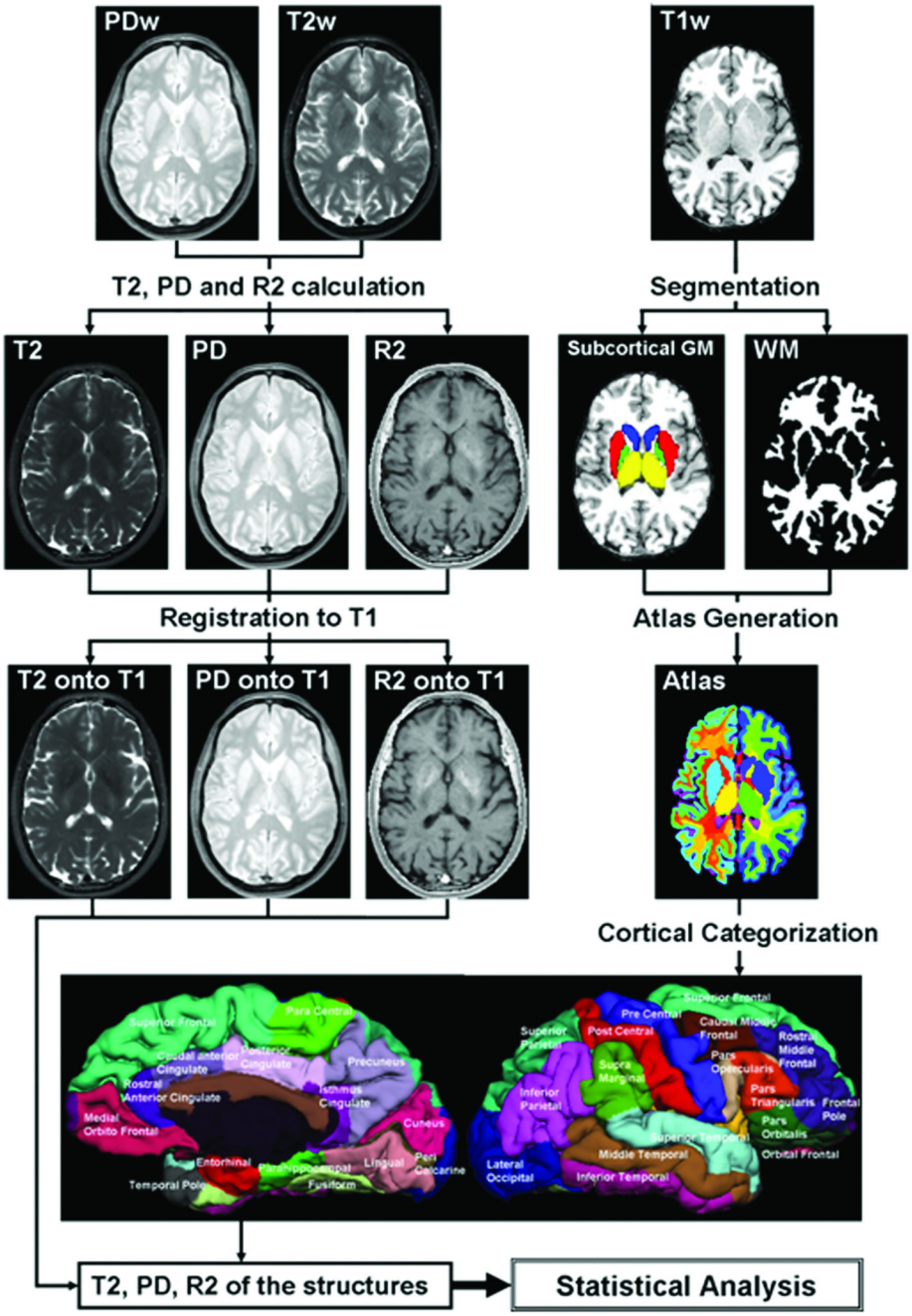

Figure 1.

A pictorial illustration of the MRI data processing pipeline used in this study. High resolution T1-weighted data were segmented and parcellated using FreeSurfer. The early and late DSE data were used to estimate T_2 relaxation time map which was aligned in each subject atlas-space. A listing of all brain regions is provided in the Supplement.

NIH-PA Author Manuscript
NIH-PA Author Manuscript
NIH-PA Author Manuscript

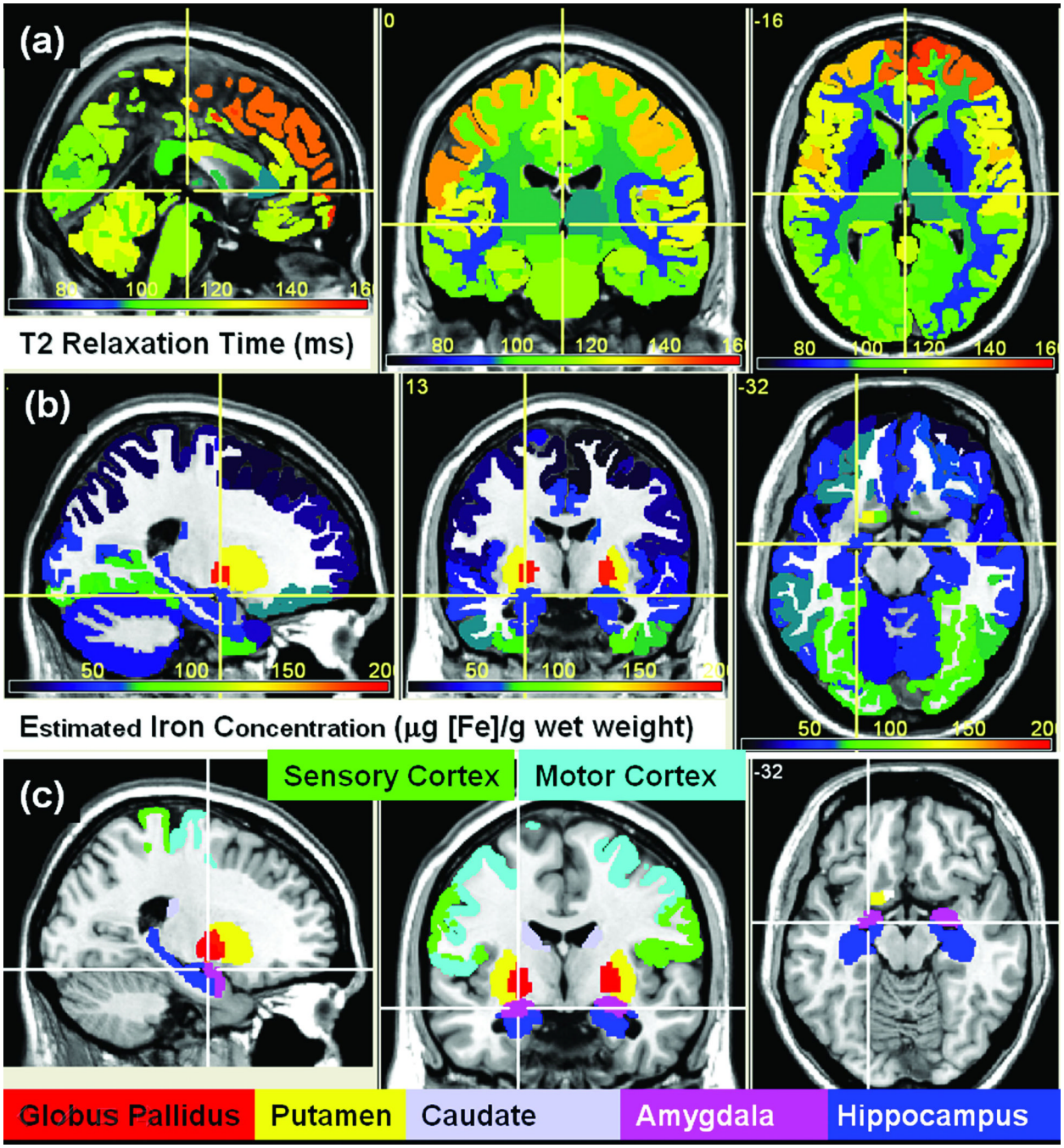

Figure 2.

(a) A visual representation of cohort means regional T_2 relaxation time (ms). Table 1 and Table 2 provide information about the average volume and T2 values. (b) Cohort average iron content map (µg [Fe]/g wet weight) estimated volume-wise using the age-projected regression of the postmortem measurements against our volume-based R_2 measurements (see Table 4). Key brain regions are shown in (c) and color coded according to the iron content values.

NIH-PA Author Manuscript
NIH-PA Author Manuscript
NIH-PA Author Manuscript

Table 1

Atlas-based bilateral volume in mL and corresponding volume-averaged T2 relaxation time of 28 gray and white matter brain regions that cover the entire brain (see Supplementary Table for a list and grouping of all brain regions).

#	Brain Structure	Volume (mL) Mean ± SD	T_2 (ms) Mean ± SD
1	Thalamus Proper	14.80 ± 1.44	95.18 ± 3.87
2	Caudate	7.21 ± 1.07	111.51 ± 7.56
3	Putamen	11.34 ± 1.34	81.64 ± 3.18
4	Globus Pallidus	3.29 ± 0.43	66.89 ± 3.29
5	Hippocampus	8.77 ± 0.81	118.56 ± 4.95
6	Amygdala	3.32 ± 0.44	112.10 ± 3.50
7	Accumbens area	1.20 ± 0.22	102.73 ± 3.88
8	Frontal Cortex	165.08 ± 18.58	134.85 ± 8.06
9	Temporal Cortex	100.95 ± 11.22	113.71 ± 3.82
10	Parietal Cortex	108.58 ± 10.93	126.62 ± 8.49
11	Occipital Cortex	41.25 ± 5.28	107.42 ± 4.54
12	Cingulate Cortex	18.27 ± 2.64	115.22 ± 4.20
13	Insular Cortex (GM)	12.09 ± 1.42	121.54 ± 4.67
14	Cerebellar Cortex (GM)	99.23 ± 11.36	121.61 ± 5.23
15	Frontal Lobe WM	144.51 ± 17.96	95.83 ± 3.15
16	Temporal Lobe WM	63.67 ± 8.30	90.71 ± 2.43
17	Parietal Lobe WM	97.16 ± 11.41	95.38 ± 3.43
18	Occipital Lobe WM	42.71 ± 6.58	96.57 ± 3.57
19	Cingulate Lobe WM	23.37 ± 2.61	93.20 ± 2.40
20	Insular WM	17.41 ± 1.70	90.22 ± 1.71
21	Cerebellar WM	29.83 ± 3.85	99.46 ± 2.50
22	Brain Stem WM	20.80 ± 2.20	113.58 ± 4.65
23	Periventricular WM	69.15 ± 13.27	96.26 ± 2.00
24	CC Anterior WM	0.82 ± 0.14	94.35 ± 4.77
25	CC Mid Anterior	0.54 ± 0.16	112.74 ± 7.73
26	CC Central	0.51 ± 0.13	115.91 ± 6.49
27	CC Mid Posterior	0.49 ± 0.10	122.39 ± 8.44
28	CC Posterior	0.93 ± 0.15	96.86 ± 4.45

NIH-PA Author Manuscript

NIH-PA Author Manuscript

NIH-PA Author Manuscript

Table 2

Atlas-based bilateral volume in mL and corresponding volume-averaged T_2 relaxation time of 12 cortical gray matter and corresponding lobar white matter subregions.

#	Brain Structure	Volume (mL) Mean ± SD	T_2 (ms) Mean ± SD
1	GM caudal middle frontal	12.75 ± 2.40	143.75 ± 11.19
2	GM precentral @ Frontal (Primary Motor)	26.77 ± 3.07	135.56 ± 10.66
3	GM entorhinal Temporal	3.17 ± 0.57	117.34 ± 5.81
4	GM postcentral @ Parietal (Primary Sensory)	18.23 ± 2.48	138.55 ± 11.09
5	GM precuneus @ Parietal	17.80 ± 2.10	115.03 ± 6.54
6	GM cuneus @ Occipital (Primary Visual Cortex)	4.79 ± 0.93	110.70 ± 7.18
7	WM caudal middle frontal	12.89 ± 2.32	97.73 ± 3.81
8	WM precentral	27.59 ± 3.39	100.37 ± 4.00
9	WM entorhinal	1.45 ± 0.38	99.77 ± 5.22
10	WM postcentral	15.00 ± 2.27	100.05 ± 4.29
11	WM precuneus	18.84 ± 2.59	93.85 ± 3.00
12	WM cuneus	5.06 ± 1.07	93.65 ± 3.41

NIH-PA Author Manuscript NIH-PA Author Manuscript NIH-PA Author Manuscript

Table 3

The parameters used for calculating regional brain iron concentration from ref. #6 using Equation [3]. The regional R_2 values are obtained from the volume-based T_2 measurements in Table 1 and Table 2. The estimated iron along with the regressed FDRI from ref #26 and the MFC from ref #20 are also listed for further analysis (see Table 4 and Figure 2).

#	Brain Region	A µg/g Wet Wt.	B Rate per year	C µg/g Wet Wt.	Extrapolated Iron Content µg/g Wet Weight. µ(σ)[a]	Current Study $R_2 = 1/T_2$ (sec $^{-1}$)	FDRI µ (σ)[b]	MFC µ (σ)[c]
1	**Globus Pallidus**	210.41	0.09	37	206.12 (9.46)	14.984 (0.720)	4.359 (0.088)	699.7 (145.0)
2	**Putamen**	140.62	0.04	46	113.87 (14.16)	12.267 (0.476)	2.363 (0.227)	387.0 (106.4)
3	**Caudate**	90.66	0.05	33	82.21 (8.38)	9.009 (0.615)	2.068 (0.146)	NA
4	**Frontal Cortex (Motor)**	40.79	0.05	40	3.13 (4.15)	7.422 (0.579)	NA	NA
5	**Prefrontal cortex (caudal middle)**	20.43	0.07	58	27.71 (1.55)	6.999 (0.552)	NA	NA
6	**Temporal Cortex (superior)**	20.70	0.07	55	29.84 (1.72)	8.076 (0.462)	NA	NA
7	**Parietal Cortex (Sensory)**	30.97	0.07	49	40.69 (2.53)	7.264 (0.581)	NA	NA
8	**Parietal Cortex (precuneus)**	30.31	0.06	60	34.67 (2.49)	8.721 (0.491)	NA	NA
9	**Occipital cortex (cuneus or visual)**	40.03	0.06	72	42.11 (3.03)	9.070 (0.562)	NA	NA
10	**Cerebellar Cortex**	20.70	0.09	68	32.10 (1.31)	8.238 (0.355)	NA	NA
11	**Thalamus**	NA	NA	NA	~60 (Fig. 8. Ref 6)	10.523 (0.415)	1.265 (0.091)	189.3 (71.6)
12	**Frontal WM (Superior)**	30.95	0.1	31.0	40.98 (1.44)	10.129 (0.405)	1.688 (0.116)	91.5 (41.9)
13	**Genu CC**	NA	NA	NA	NA	10.626 (0.535)	1.239 (0.066)	174.1(45.5)
14	**Splenium CC**	NA	NA	NA	NA	10.345 (0.460)	0.970 (0.06	103.0 (34.4)
15	**Hippocampus**	NA	NA	NA	NA	8.449 (0.347)	0.689 (0.029)	NA

*(a)*The A, B and C values were obtained from the best fit postmortem iron content or [Fe] vs. age data in Hallgren and Sourander paper (Ref 6; N=81; age = 0–100 years; Ref 6). Mean and standard deviation values of age-expected iron content for all our subjects (n=1 to N=86). Iron content was estimated for each subject n and region r as **Iron (n, r) = A(n) * [1-exp (−B(r)*Age(n))] + C(r)**. The average iron content in the thalamus (TH) was estimated from Fig. 8 in Ref. 6.

*(b)*Computed mean and standard deviation for each subject in our cohort based on the age-regressed FDRI data on both men and women in Bartzokis et al. (Ref 24).

*(c)*Based on the tabulated magnetic field correlation (MFC) data on 14 healthy controls (N=14; mean age = 39 & range 23–55 years) in Ge et al. (Ref 20).

NIH-PA Author Manuscript NIH-PA Author Manuscript NIH-PA Author Manuscript

Magn Reson Med. Author manuscript; available in PMC 2013 March 1.

Table 4

Pearson correlation coefficient (r) and statistical significance (p) of R_2 vs. estimated iron (see Table 1) and the correspondence between FDRI, MFC, R_2 and estimated iron. The r and p values are listed for several combinations of brain regions.

Linear Fit Model	Number of brain regions (*I, II, III*)	Intercept α (S.D)	Slope β (S.D)	Pearson Correlation r	Correlation Significance p
Iron vs. R_2[a]	12 included (eS+Crtx+Fwm+TH)	6.835 (0.480)	0.041 (0.006)	0.906	**4.8×10^{-5}**
Iron vs. R_2[a]	10 excluded (TH, Fwm)	6.444 (0.412)	0.042 (0.005)	0.951	**2.4×10^{-5}**
Iron vs. R_2[a]	9 excluded (CN; Fwm, TH)	6.507 (0.405)	0.043 (0.005)	0.959	**4.3×10^{-5}**
Iron vs. R_2[a]	8 excluded (CN, cuneus; Fwm, TH)	6.371 (0.427)	0.044 (0.005)	0.965	**1.0×10^{-4}**
Iron vs. R_2[a]	7 excluded (CN, cuneus, precuneus; Fwm, TH)	6.172 (0.447)	0.045 (0.005)	0.973	**2.3×10^{-4}**
Iron vs. R_2[a]	7 excluded (eS; Fwm, TH)	7.226 (1.983)	0.021 (0.055)	0.168	0.720
FDRI vs. R_2[b]	8 included (eS, HC; Fwm, TH, gCC, sCC)	8.014 (0.766)	1.517 (0.360)	0.865	**0.006**
FDRI vs. R_2[b]	7 excluded (CN)	8.209 (0.449)	1.579 (0.210)	0.959	**6.6×10^{-4}**
FDRI vs. R_2[b]	5 excluded (CN, TH, Fwm)	8.289 (0.529)	1.583 (0.225)	0.971	**0.006**
R_2vs. MFC[c]	6 included (GP, PT; Fwm, TH, gCC, sCC)	9.288 (0.137)	0.008 (0.000)	0.995	**3.5×10^{-5}**
Iron vs.FDRI[d]	5 included (DGM; Fwm, TH)	0.552 (0.31)	0.018 (0.003)	0.968	**0.007**
Iron vs. MFC[e]	4 included (GP, PT; Fwm, TH)	−39.178 (17.824)	3.621 (0.145)	0.998	**0.002**
FDRI vs. MFC[f]	5 included (GP, PT; Fwm, TH, gCC, sCC)	−39.856 (17.284)	171.869 (7.219)	0.997	**1.6×10^{-4}**

I Abbreviations: CN = Caudate Nuclei; Fwm= Frontal white matter; gCC, sCC = genu and splenium of the corpsus callosum; GP = Globus Pallidus; HC = Hippocampus; PT = Putamen; TH = Thalamus Proper; eS = extended striatum = GP + PT + CN.

II Iron refers to the regional brain [Fe] concentration of our cohort estimated from Hallgren and Sourander data which did not include splenium CC, genu CC, or Hippocampus (see Table 3). The R_2, FDRI and MFC average values of the selected brain regions are provided in Table 3.

III The linear regression models tested are (see Methods):

(a) $R_2\ (\sec^{-1}) = \alpha(\sec^{-1}) + \beta\ (\sec^{-1}/(\mu g\ Fe/g\ ww))^*$ [Iron Content]

(b) $R_2 = \alpha_1\beta_1 * FDRI$

(c) $R_2 = \alpha_2 + \beta_2 * MFC$

NIH-PA Author Manuscript

NIH-PA Author Manuscript

NIH-PA Author Manuscript

(d) $\text{FDRI} = \alpha_3 + \beta_3 * [\text{Fe}]$;

(e) $\text{MFC} = \alpha_4 + \beta_4 * [\text{Fe}]$(Iron content units are μg [Fe]/g Wet Weight)

(f) $\text{MFC} = \alpha_5 + \beta_5 * \text{FDRI}$